Fate of the Fermi surface coupled to a single-wave-vector cavity mode

Bernhard Frank, Michele Pini, Johannes Lang, Francesco Piazza

Angaben zur Veröffentlichung / Publication details:

Frank, Bernhard, Michele Pini, Johannes Lang, and Francesco Piazza. 2026. "Fate of the Fermi surface coupled to a single-wave-vector cavity mode." *Physical Review Letters* 136 (14): 143403. https://doi.org/10.1103/t4xb-6x3z.

Fate of the Fermi Surface Coupled to a Single-Wave-Vector Cavity Mode

Bernhard Frank,[1] Michele Pini,[2,3,*] Johannes Lang,[4] and Francesco Piazza[2,3]
[1]Institut für Theoretische Physik and Würzburg-Dresden Cluster of Excellence ct.qmat, Technische Universität Dresden, 01062 Dresden, Germany
[2]Theoretical Physics III, Center for Electronic Correlations and Magnetism, Institute of Physics, University of Augsburg, 86135 Augsburg, Germany
[3]Max-Planck-Institut für Physik komplexer Systeme, 01187 Dresden, Germany
[4]Institut für Theoretische Physik, Universität zu Köln, 50937 Cologne, Germany

(Received 16 May 2025; revised 18 December 2025; accepted 12 March 2026; published 10 April 2026)

The electromagnetic field of standing-wave or ring cavities induces a spatially modulated, infinite-range interaction between atoms in an ultracold Fermi gas, with a single wavelength comparable to the Fermi length. This interaction has no analog in other systems of itinerant particles and has so far been studied only in the regime where it is attractive at zero distance. Here, we fully solve the problem of competing instabilities of the Fermi surface induced by single-wavelength interactions. We find that while the density-wave (superradiant) instability dominates on the attractive side, it is absent for repulsive interactions, where the competition is instead won by nonsuperradiant superfluid phases at low temperatures, with fermion pairs forming at both vanishing and finite center-of-mass momentum. Moreover, even in the absence of such symmetry-breaking instabilities, the Fermi surface exhibits a peculiar anisotropic deformation. We estimate this full phenomenology to be within reach of dedicated state-of-the-art experimental setups.

DOI: 10.1103/t4xb-6x3z

Introduction—The problem of an electron gas coupled to transverse photons is a longstanding one in many-body physics [1], showing an intriguing phenomenology deviating from standard metallic behavior. Recent developments in the field of cavity quantum materials [2] promise to bring this rich physics within experimental reach [3], owing to the enhancement of the light-matter coupling via optical confinement. The latter introduces a tunable gap; it closes at the superradiant phase transition, where non-Fermi-liquid behavior has indeed been predicted [4].

Light confinement via mirrors enables strong coupling of matter to a single electromagnetic mode. In solids, the wavelength of this mode is orders of magnitude larger than the Fermi length [5,6]. By contrast, in ultracold atomic systems, where electrons are replaced by neutral fermionic atoms, these two scales can be comparable [7]. This gives access to a new regime where the photon-mediated interaction transfers a single, but finite momentum between fermions, set by the cavity-photon wave vector. This situation, absent in other itinerant systems, becomes particularly interesting in the presence of a Fermi surface (FS).

To date, both theory [8–16] and experiment [17–19] have mainly focused on the attractive regime, where the superradiant (SR) (density wave) phase dominates due to a collective enhancement caused by the single-wave-vector nature of the photon-mediated interaction. In this work, we

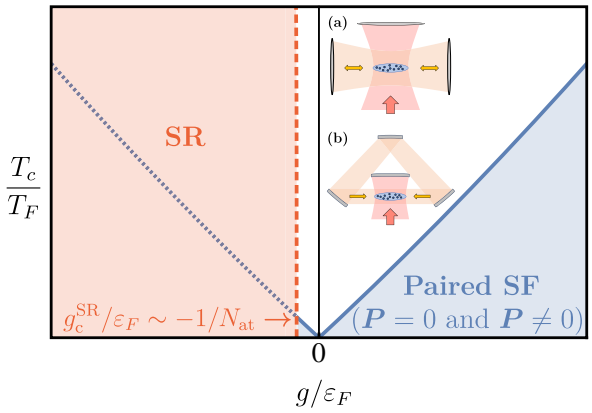

FIG. 1. Phase diagram for a transversely driven ultracold polarized Fermi gas in a cavity. For attractive interactions ($g < 0$), below a critical coupling scaling as the inverse of the number of atoms, the system is dominated by a superradiant (SR) phase with modulated density ordering in the atom cloud. For repulsive interactions ($g > 0$), the SR phase is suppressed, and a paired superfluid (SF) phase emerges with a superposition of pairs with zero and finite c.m. momentum $\boldsymbol{P}$. Inset: sketch of two possible cavity geometries, (a) a standing-wave cavity and (b) a ring cavity.

*Contact author: michele.pini@uni-a.de

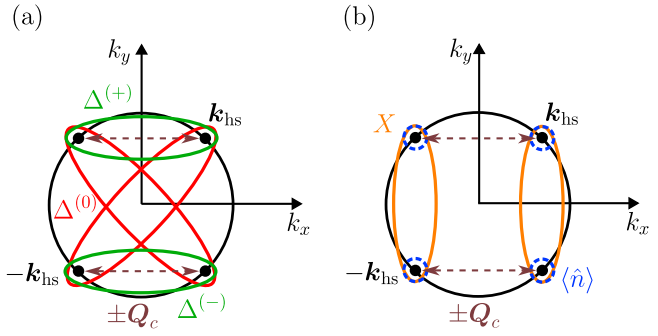

FIG. 2. Sketch of the mean-field decouplings evaluated at the hot spots on the FS. (a) Cooper order parameters $\Delta^{(0)}_{\boldsymbol{k}_{\rm hs}} = g\langle\hat{c}_{-\boldsymbol{k}_{\rm hs}}\hat{c}_{\boldsymbol{k}_{\rm hs}}\rangle$ and $\Delta^{(0)}_{\boldsymbol{k}_{\rm hs}-\boldsymbol{Q}_c} = g\langle\hat{c}_{-\boldsymbol{k}_{\rm hs}+\boldsymbol{Q}_c}\hat{c}_{\boldsymbol{k}_{\rm hs}-\boldsymbol{Q}_c}\rangle$ (red), together with PDW order parameters $\Delta^{(\pm)}_{\pm(\boldsymbol{k}_{\rm hs}-\boldsymbol{Q}_c)} = \langle\hat{c}_{\pm\boldsymbol{k}_{\rm hs}}\hat{c}_{\pm(\boldsymbol{k}_{\rm hs}-\boldsymbol{Q}_c)}\rangle$ (green). (b) Exciton order parameters $X_{\pm\boldsymbol{k}_{\rm hs}} = g\langle\hat{c}^\dagger_{\pm\boldsymbol{k}_{\rm hs}}\hat{c}_{\mp(\boldsymbol{k}_{\rm hs}-\boldsymbol{Q}_c)}\rangle$ (orange), together with momentum occupation numbers $\langle\hat{n}_{\pm\boldsymbol{k}_{\rm hs}}\rangle = \langle\hat{c}^\dagger_{\pm\boldsymbol{k}_{\rm hs}}\hat{c}_{\pm\boldsymbol{k}_{\rm hs}}\rangle$ and $\langle\hat{n}_{\pm(\boldsymbol{k}_{\rm hs}-\boldsymbol{Q}_c)}\rangle = \langle\hat{c}^\dagger_{\pm(\boldsymbol{k}_{\rm hs}-\boldsymbol{Q}_c)}\hat{c}_{\pm(\boldsymbol{k}_{\rm hs}-\boldsymbol{Q}_c)}\rangle$ (blue dashed). The latter are at the origin of the FS deformation (see Fig. 3), whereas the others are associated with instabilities due to spontaneous symmetry breaking. (a) Pairing channel. (b) Exchange channel.

leverage the latter feature to fully solve the competition problem via a mean-field treatment, which becomes exact in the thermodynamic limit [20].

As shown in Fig. 1, on the repulsive side of the photon-mediated interaction, the SR phase is absent, giving way to a nontrivial competition between nonsuperradiant phases, governed by the hot spot points on the FS which are connected by a photon wave vector (see Fig. 2). At low temperatures, this competition is won by superfluid phases, which exhibit degenerate pairing channels with either vanishing or finite center-of-mass (c.m.) momentum. Remarkably, independent of the sign of the interaction and even in the absence of symmetry breaking, we find that the Fermi surface is always anisotropically deformed. This deformation is a true many-body effect due to the anisotropy of photon-mediated interactions, similarly to what happens in dipolar Fermi gases [21–23]. Contrary to the latter case, however, the FS is not an ellipsoid, but rather shows a new type of deformation geometry due to the single-wave-vector nature of the interaction.

We fully characterize the behavior of the pairing gap, which strongly depends on momentum, and estimate that the required temperature and light-matter couplings lie within reach of dedicated, state-of-the-art experimental setups.

Model—We study a fully spin-polarized ultracold gas of fermionic atoms, at temperature T, confined by an external potential to two spatial dimensions [24] in a homogeneous trap [25,26]. Because of spin polarization, intrinsic short-range interactions are absent [24,27,28], allowing us to focus exclusively on photon-mediated interactions.

The dispersion relation is given by the standard form $\xi_{\boldsymbol{k}} = \boldsymbol{k}^2/(2m) - \varepsilon_F$ (we work in units with $\hbar = k_B = 1$), where the Fermi energy ε_F determines the particle density $n = k_F^2/(4\pi)$ via the Fermi wave vector $k_F = (2m\varepsilon_F)^{1/2}$, which sets the radius of the Fermi disk in the absence of interactions at zero temperature. The Fermi gas is located within an optical ring cavity [Fig. 1(b)] that supports two counterpropagating cavity modes $\exp(\pm i\boldsymbol{Q}_c\cdot\boldsymbol{r})$ with cavity momentum $\boldsymbol{Q}_c$ and corresponding frequency ω_c, and transversally driven by a laser pump of frequency ω_p, with an adjustable detuning $\Delta_c = \omega_c - \omega_p$ [29,30]. Typical cavity experiments with ultracold Fermi gases [17–19] operate at densities where k_F and Q_c are of comparable magnitude. Here we focus on a ring cavity, which is translationally invariant and thus the simplest case. However, we find similar results for the experimentally more common standing-wave cavity [see Fig. 1(a)]; a summary of this generalization is provided below and discussed in full in Supplemental Material [31]. In the dispersive regime, the system is described by the Hamiltonian [7]

$$\hat{H} = \sum_{\boldsymbol{k}}\xi_{\boldsymbol{k}}\hat{c}^\dagger_{\boldsymbol{k}}\hat{c}_{\boldsymbol{k}} + \frac{g}{2}\sum_{\substack{\boldsymbol{p},\boldsymbol{k}\\ s=\pm1}}\hat{c}^\dagger_{\boldsymbol{p}+s\boldsymbol{Q}_c}\hat{c}^\dagger_{\boldsymbol{k}-s\boldsymbol{Q}_c}\hat{c}_{\boldsymbol{k}}\hat{c}_{\boldsymbol{p}}, \qquad (1)$$

where the geometry of the ring cavity implies momentum conservation in the interaction term. In the above, the operators $\hat{c}_{\boldsymbol{k}}$ and $\hat{c}^\dagger_{\boldsymbol{k}}$ annihilate and create a fermion with momentum $\boldsymbol{k}$. Assuming $|\Delta_c|$ much larger than the cavity loss rate κ, the tunable coupling strength is given by $g \approx U_0V_0/\Delta_c$, where U_0 is the depth of the cavity potential per photon and V_0 corresponds to the light shift induced by the pump, proportional to the pump intensity [7,18,34].

Physically, these cavity-mediated interactions transfer only fixed momenta $\pm\boldsymbol{Q}_c$ and are therefore of infinite range in real space, with a periodic modulation with wave vector $\boldsymbol{Q}_c$. The sign of g, which is tunable via the cavity detuning Δ_c, determines the sign of the interaction at zero distance. Because of the long-range nature of the interactions, mean-field theory becomes exact in the thermodynamic limit [7], which forms the basis of the analysis of the phase diagram below.

Mean-field analysis—We first identify the most relevant low-energy processes in the pairing and exchange channel [35], since the direct channel is dominated by the density wave (superradiance). For a given $\boldsymbol{Q}_c$ with $Q_c \sim k_F$ and $Q_c < 2k_F$ (necessary for hot spots to exist), the Hamiltonian $\hat{H}$ singles out special interaction processes where all incoming *and* outgoing momentum states reside on the FS, which, therefore, correspond to the primary candidates for instabilities. As depicted in Fig. 2, these occur if and only if the four momentum hot spots $\pm\boldsymbol{k}_{\rm hs}$ and $\pm(\boldsymbol{k}_{\rm hs} - \boldsymbol{Q}_c)$ are involved.

In $\hat{H}$, these two processes are given by the contributions

$$g\hat{c}^{\dagger}_{\boldsymbol{k}_{\rm hs}-\boldsymbol{Q}_c}\hat{c}^{\dagger}_{-\boldsymbol{k}_{\rm hs}+\boldsymbol{Q}_c}\hat{c}_{-\boldsymbol{k}_{\rm hs}}\hat{c}_{\boldsymbol{k}_{\rm hs}}, \tag{2}$$

$$g\hat{c}^{\dagger}_{\pm(\boldsymbol{k}_{\rm hs}-\boldsymbol{Q}_c)}\hat{c}^{\dagger}_{\pm\boldsymbol{k}_{\rm hs}}\hat{c}_{\pm(\boldsymbol{k}_{\rm hs}-\boldsymbol{Q}_c)}\hat{c}_{\pm\boldsymbol{k}_{\rm hs}}. \tag{3}$$

A standard mean-field decoupling of Eq. (2) in both the pairing and the exchange channel yields $g\hat{c}^{\dagger}_{\boldsymbol{k}_{\rm hs}-\boldsymbol{Q}_c}\hat{c}^{\dagger}_{-\boldsymbol{k}_{\rm hs}+\boldsymbol{Q}_c}\hat{c}_{-\boldsymbol{k}_{\rm hs}}\hat{c}_{\boldsymbol{k}_{\rm hs}} \simeq \bar{\Delta}^{(0)}_{\boldsymbol{k}_{\rm hs}-\boldsymbol{Q}_c}\hat{c}_{-\boldsymbol{k}_{\rm hs}}\hat{c}_{\boldsymbol{k}_{\rm hs}} - \bar{X}_{-\boldsymbol{k}_{\rm hs}}\hat{c}^{\dagger}_{-\boldsymbol{k}_{\rm hs}+\boldsymbol{Q}_c}\hat{c}_{\boldsymbol{k}_{\rm hs}} + \text{H.c.} + \text{const.}$ Here, a finite value of $\Delta^{(0)}_{\boldsymbol{k}_{\rm hs}} = g\langle\hat{c}_{-\boldsymbol{k}_{\rm hs}}\hat{c}_{\boldsymbol{k}_{\rm hs}}\rangle$ [red in Fig. 2(a)] describes a state with pairs of vanishing c.m. momentum, which is referred to as Cooper pairing in the following. On the other hand, for the exchange channel, the particle-hole expectation value $X_{-\boldsymbol{k}_{\rm hs}} \equiv g\langle c^{\dagger}_{-\boldsymbol{k}_{\rm hs}}c_{\boldsymbol{k}_{\rm hs}-\boldsymbol{Q}_c}\rangle$ [orange in Fig. 2(b)] describes exciton condensation (XCON) with finite relative momentum $\boldsymbol{K} = 2\boldsymbol{k}_{\rm hs} - \boldsymbol{Q}_c$. Applying the same decoupling to process (3) leads to $g\hat{c}^{\dagger}_{\pm(\boldsymbol{k}_{\rm hs}-\boldsymbol{Q}_c)}\hat{c}^{\dagger}_{\pm\boldsymbol{k}_{\rm hs}}\hat{c}_{\pm(\boldsymbol{k}_{\rm hs}-\boldsymbol{Q}_c)}\hat{c}_{\pm\boldsymbol{k}_{\rm hs}} \simeq \bar{\Delta}^{(\pm)}_{\pm(\boldsymbol{k}_{\rm hs}-\boldsymbol{Q}_c)}\hat{c}_{\pm(\boldsymbol{k}_{\rm hs}-\boldsymbol{Q}_c)}\hat{c}_{\pm\boldsymbol{k}_{\rm hs}} - g\langle\hat{n}_{\pm(\boldsymbol{k}_{\rm hs}-\boldsymbol{Q}_c)}\rangle\hat{c}^{\dagger}_{\pm\boldsymbol{k}_{\rm hs}}\hat{c}_{\pm\boldsymbol{k}_{\rm hs}} + \text{H.c.} + \text{const.}$ The order parameter $\Delta^{(\pm)}_{\pm(\boldsymbol{k}_{\rm hs}-\boldsymbol{Q}_c)} = \langle\hat{c}_{\pm\boldsymbol{k}_{\rm hs}}\hat{c}_{\pm(\boldsymbol{k}_{\rm hs}-\boldsymbol{Q}_c)}\rangle$ [green in Fig. 2(a)] describes pair-density-wave (PDW) pairing with fixed c.m. momentum $\pm\boldsymbol{P} = \pm(2\boldsymbol{k}_{\rm hs} - \boldsymbol{Q}_c)$. In the exchange channel, momentum occupation numbers $\langle\hat{n}_{\boldsymbol{k}_{\rm hs}}\rangle = \langle\hat{c}^{\dagger}_{\boldsymbol{k}_{\rm hs}}\hat{c}_{\boldsymbol{k}_{\rm hs}}\rangle$ [blue dashed in Fig. 2(b)] emerge, which do not give rise to instabilities but instead lead to a reshaping of the FS. Moreover, as we shall see below, the pairing instabilities $\Delta^{(0,\pm)}$ are always dominant over the XCON instability.

To extend the mean-field approach beyond the hot spots, we introduce the momentum deviations $\boldsymbol{\delta k}^{\pm} = (\pm\delta k_x, \delta k_y)$ and include shifted copies of the hot spots, displaced by multiples of $\boldsymbol{Q}_c$. The generalized pairing order parameters then become ($l \in \mathbb{Z}$)

$$\begin{aligned}
\Delta^{(0)}_{\boldsymbol{k}_{\rm hs}+\boldsymbol{\delta k}^{\pm}+l\boldsymbol{Q}_c} &\equiv g\langle\hat{c}_{-(\boldsymbol{k}_{\rm hs}+\boldsymbol{\delta k}^{\pm}+l\boldsymbol{Q}_c)}\hat{c}_{\boldsymbol{k}_{\rm hs}+\boldsymbol{\delta k}^{\pm}+l\boldsymbol{Q}_c}\rangle \\
\Delta^{(+)}_{\boldsymbol{k}_{\rm hs}+\boldsymbol{\delta k}^{+}+l\boldsymbol{Q}_c} &\equiv g\langle\hat{c}_{\boldsymbol{k}_{\rm hs}+\boldsymbol{\delta k}^{-}-(l+1)\boldsymbol{Q}_c}\hat{c}_{\boldsymbol{k}_{\rm hs}+\boldsymbol{\delta k}^{+}+l\boldsymbol{Q}_c}\rangle \\
\Delta^{(-)}_{-\boldsymbol{k}_{\rm hs}-\boldsymbol{\delta k}^{+}+l\boldsymbol{Q}_c} &\equiv g\langle\hat{c}_{-\boldsymbol{k}_{\rm hs}-\boldsymbol{\delta k}^{+}-(l-1)\boldsymbol{Q}_c}\hat{c}_{-\boldsymbol{k}_{\rm hs}-\boldsymbol{\delta k}^{-}+l\boldsymbol{Q}_c}\rangle.
\end{aligned} \tag{4}$$

Further details—including the analogous expressions for the exchange channels X, Y [the latter becomes distinct only beyond the hot spots, see Eq. (B8)], and $\langle\hat{n}\rangle$—are presented in the End Matter (EM), along with the full mean-field Hamiltonian. Moreover, the Hamiltonian (1) exhibits a special SO(2) symmetry in momentum space originating from the fact that the k_y components ($\hat{\boldsymbol{e}}_y \perp \boldsymbol{Q}_c$) are untouched by the interaction, such that any fermion may be replaced by a superposition with the fermion with flipped k_y momentum. This leads to an exact degeneracy between Cooper and PDW pairing, as is detailed in the EM, too. Upon entering the paired phase, the system spontaneously breaks this symmetry by selecting a specific superposition of Cooper and PDW states.

Given the full mean-field decoupled Hamiltonian, one can derive (see EM) a closed set of coupled equations for all the above order parameters, which we use to solve the full problem of competing instabilities.

Results—We focus on repulsive interactions, $g > 0$, such that the superradiant density wave instability (direct channel) is absent (see EM for details). To fully solve the coupled mean-field equations (B13), we resort to numerics on a truncated momentum grid containing the vicinity of the Fermi sea and the corresponding momenta shifted by $\pm\boldsymbol{Q}_c$. Including further shifted copies amounts to a perturbative expansion in g/ϵ_F, yielding small corrections in the regime $|g|/\varepsilon_F \ll 1$. The results in Figs. 3 and 4 are shown for $g = 0.3\epsilon_F$ and $Q_c = 1.2k_F$.

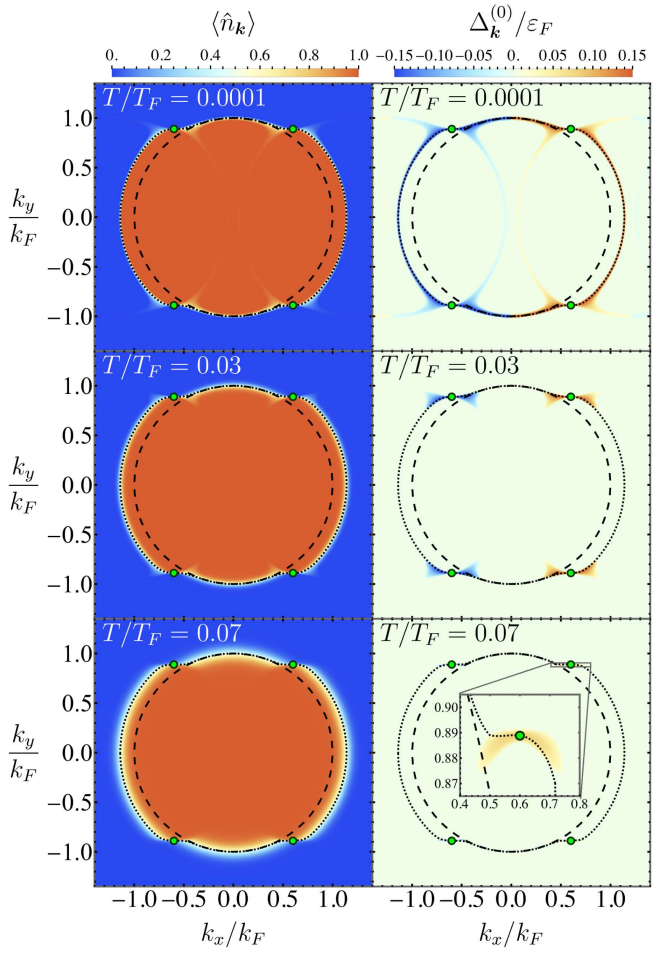

FIG. 3. Momentum distribution $\langle\hat{n}_{\boldsymbol{k}}\rangle$ (left) and Cooper gap $\Delta^{(0)}_{\boldsymbol{k}}$ (right) for different temperatures below T_c. Dotted line: FS reshaped by interactions. The dotted arches on the left and right side correspond to the analytic result $\xi_{\boldsymbol{k}} = g$. Dashed line: bare FS. Green dots: renormalized hot spots. Inset in the lower-right panel: enlarged view of the region around a hot spot for a temperature just below T_c.

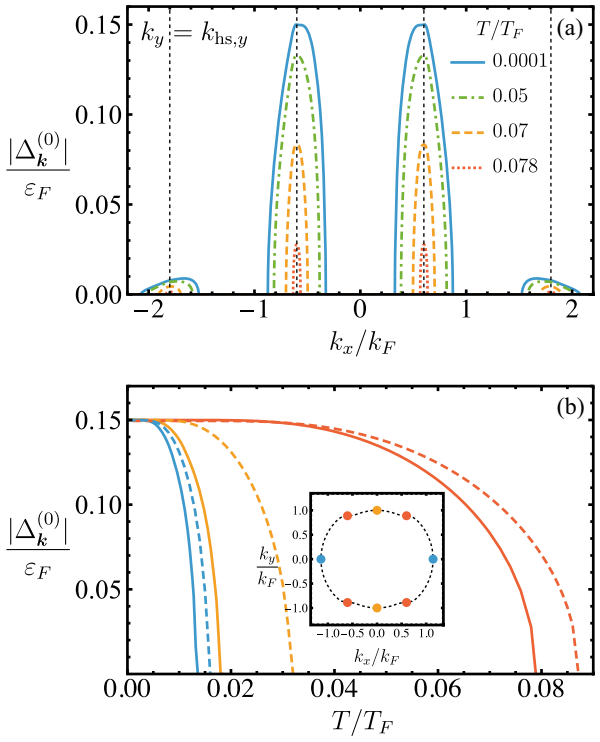

FIG. 4. (a) $|\Delta_{\boldsymbol{k}}^{(0)}|$ as a function of k_x along a horizontal momentum cut passing through the hot spots ($k_y = k_{\mathrm{hs},y}$) at different temperatures below T_c. The dashed vertical lines correspond to the k_x of the hot spots and their first shifted copies. (b) $|\Delta_{\boldsymbol{k}}^{(0)}|$ as a function of temperature T for ring (solid lines) and standing-wave (dashed lines) cavities at specific $\boldsymbol{k}$ points on the FS. For the ring cavity, these are indicated with dots of the corresponding color in the inset (hot spots shown in red). The standing-wave cavity calculation has been performed on the equivalent points of the circular FS.

To gain a deeper understanding of the underlying physics, we first analyze the mean-field equations in the absence of pairing and exchange. The Hamiltonian then becomes diagonal with a renormalized dispersion, and the self-consistency equation reduces to

$$\epsilon_{\boldsymbol{k}}^{(\hat{n})} = \xi_{\boldsymbol{k}} - g\sum_{s=\pm 1}\langle \hat{n}_{\boldsymbol{k}+s\boldsymbol{Q}_c}\rangle \qquad \langle \hat{n}_{\boldsymbol{k}}\rangle = n_F(\epsilon_{\boldsymbol{k}}^{(\hat{n})}), \quad (5)$$

with the Fermi-Dirac distribution n_F. This results in a reshaped FS: From a grand-canonical perspective, the ground-state corresponds to a Fermi sea that includes all single-particle states with $\epsilon_{\boldsymbol{k}}^{(\hat{n})} < 0$. For $g > 0$ (see Ref. [31] for the case $g < 0$), Equation (5) implies that not only the noninteracting FS $\xi_{\boldsymbol{k}} < 0$ is occupied, but also momentum states with $\xi_{\boldsymbol{k}} - g < 0$, provided that simultaneously $\xi_{\boldsymbol{k}\pm\boldsymbol{Q}_c} - g < 0$. The left column of Fig. 3 shows the reshaped FS with renormalized hot spots (green dots) for three different temperatures below T_c. The new $k_{\mathrm{hs},y}$ hot spot coordinates are determined by the equation $\xi_{\boldsymbol{k}_{\mathrm{hs}}} = g$ (hot spots on reshaped FS), where $k_{\mathrm{hs},x} = \pm Q_c/2$ because of the symmetry $k_x \leftrightarrow -k_x$. For the parameters used, this predicts the hot spots at $(\pm 0.6k_F, \pm 0.889k_F)$, in perfect agreement with the numerics.

We can now use the mean-field equations (restricted to the renormalized hot spots) to separately determine the critical temperatures for Cooper and PDW instabilities, yielding

$$T_c^{(0)} = T_c^{(\pm)} = \frac{|g|}{4} + \frac{g^2}{8\epsilon_{\boldsymbol{k}_{\mathrm{hs}}+\boldsymbol{Q}_c}^{(\hat{n})}} + \mathcal{O}(|g|^3/\varepsilon_F^2), \quad (6)$$

whereas for the XCON sector one obtains

$$T_c^{(X)} = \frac{|g|}{4} + |g|e^{-4\epsilon_{\boldsymbol{k}_{\mathrm{hs}}+\boldsymbol{Q}_c}^{(\hat{n})}/|g|} + \ldots, \quad (7)$$

where we give the leading exponential correction. The linear dependence on g also appears in other models with fixed momentum transfer [5,6,32]. However, in our case where this fixed momentum is also strictly nonzero, T_c becomes independent of the sign of g, since any initial state has to undergo an even number of scattering events to return to itself: e.g., in the Cooper channel $(\boldsymbol{k}_{\mathrm{hs}}, -\boldsymbol{k}_{\mathrm{hs}}) \xrightarrow{g} (\boldsymbol{k}_{\mathrm{hs}} - \boldsymbol{Q}_c, -\boldsymbol{k}_{\mathrm{hs}} + \boldsymbol{Q}_c) \xrightarrow{g} (\boldsymbol{k}_{\mathrm{hs}}, -\boldsymbol{k}_{\mathrm{hs}})$. As a consequence, all the nonsuperradiant instabilities occur for both attractive and repulsive interactions, as shown in Fig. 1. Because of the symmetry (B1), Cooper pairing and PDW states are degenerate, as the results for T_c confirm. Since the degeneracy follows from a symmetry of the microscopic Hamiltonian, it is exact and will not be lifted upon the inclusion of higher orders or fluctuations. Comparison of Eqs. (6) and (7) shows that pairing always dominates in the relevant experimental regime $\epsilon_{\boldsymbol{k}_{\mathrm{hs}}+\boldsymbol{Q}_c} \sim \varepsilon_F$ and $|g|/\varepsilon_F \ll 1$ due to the next-to-leading order terms. These arise from the first shifted copies of the hot spots and explain the suppression of XCON: To create a particle-particle pair, only the necessary energy to scatter from the FS to the shifted copies is required. In contrast, the particle-hole pair in the case of XCON needs, in addition, a thermally excited particle at the shifted copy that turns into the hole. At low T, such an excited state has an exponentially small probability. This has also been confirmed in the numerics: By initializing the system in a generic superposition of Cooper, PDW, and XCON order parameters, the iterative calculation always converges to a state where the XCON is suppressed. For this reason, in the following, we focus only on the dominant pairing channels.

The right column of Fig. 3 depicts the pairing gap $\Delta_{\boldsymbol{k}}^{(0)} = g\langle \hat{c}_{-\boldsymbol{k}}\hat{c}_{\boldsymbol{k}}\rangle$ for three different temperatures. Because of the symmetry-induced degeneracy, $\Delta_{\boldsymbol{k}}^{(\pm)}$ is identical. The critical temperature corresponds to the instability at the hot spots, and pairing progressively gaps the FS as the temperature is lowered. The sign structure of $\Delta_{\boldsymbol{k}}^{(0)}$ is due to the form

of the mean-field equations (see EM) and the triplet nature of the pairing: under $\boldsymbol{k} \to -\boldsymbol{k}$, the pairing amplitude $\langle \hat{c}_{-\boldsymbol{k}} \hat{c}_{\boldsymbol{k}} \rangle$ changes sign due to the fermionic anticommutation.

In Fig. 4(a) we plot $\Delta_{\boldsymbol{k}}^{(0)}$ at fixed $k_y = k_{\mathrm{hs},y}$: The maxima of the order parameter occur at the hot spots while side peaks are found in the vicinity of the shifted copies. Both the variation of $\Delta^{(0)}$ around $\boldsymbol{k}_{\mathrm{hs}}$, as well as the reduction of the maximum from $\boldsymbol{k}_{\mathrm{hs}}$ to the shifted copy depend algebraically on g and $\xi_{\boldsymbol{k}_{\mathrm{hs}}+\boldsymbol{Q}_c}$ (see EM). Furthermore, analytics at $T = 0$ provide the gap value $|\Delta_{\boldsymbol{k}}^{(0,\pm)}(T \to 0)| = |g|/2$ everywhere on the reshaped FS, in agreement with Figs. 3 and 4(a). Figure 4(b) shows the dependence of $\Delta_{\boldsymbol{k}}^{(0)}$ on the temperature for different momenta on the FS. The blue dotted line corresponds to temperatures where the full FS is gapped. The evaluation of Eq. (6) for our parameters yields $T_c^{(0)} = 0.0789 T_F$ again in perfect agreement with Fig. 4(b).

Standing-wave cavity—On top of the momentum-conserving interactions in Eq. (1), the standing-wave-cavity setup exhibits additional interactions that break momentum conservation and change the c.m. momentum of any pair by $\pm 2\boldsymbol{Q}_c$. Nevertheless, analogous derivations lead to similar conclusions (see Ref. [31] for details). Again, pairing dominates over the exchange channel. However, now a third type of leading pairing instability occurs, which arises from pairs of the form $\Delta_{\boldsymbol{k}_{\mathrm{hs}}}^{(\|)} = g\langle \hat{c}_{-\boldsymbol{k}_{\mathrm{hs}}+\boldsymbol{Q}_c} \hat{c}_{\boldsymbol{k}_{\mathrm{hs}}} \rangle$. It is related to $\Delta^{(0)}$ pairs by an additional SO(2) symmetry of a form analogous to Eq. (B1) with different momentum indices, while the latter symmetry also remains intact. As a result, $\Delta^{(0)}$, $\Delta^{(\pm)}$, and $\Delta^{(\|)}$ pairs are all exactly degenerate, independently of the mean-field approximation. The critical temperature is derived as $T_c = |g|/4 + 3g^2/(8\epsilon_{\boldsymbol{k}_{\mathrm{hs}}+\boldsymbol{Q}_c}^{(\hat{n})}) + \mathcal{O}(|g|^3/\varepsilon_F^2)$, where the g^2 correction is enhanced by a factor of 3 with respect to Eq. (6), owing to pairs connected to the hot spots via nonmomentum-conserving interactions. This result, as well as the symmetry-induced degeneracy, is confirmed numerically [see Fig. 4(b)]. Consequently, the phase diagram of Fig. 1 applies to both cavity geometries.

Experimental parameters considerations—Our predictions are general and do not rely on a specific atomic species; multiple choices of fermions and cavity configurations may be explored to optimize parameters. To compare with the present state of the art, we focus on the commonly used choice of ^{6}Li [17–19,36]. The key requirement for observing the predicted phase transition, based on the leading order of Eq. (6) for T_c, is the dimensionless ratio $|g|/4T > 1$, where $g \approx U_0 V_0/\Delta_c$ [see below Eq. (1)]. Present experiments typically operate with $U_0/h \approx 10$–20 Hz [18,19,36], while the pump-induced light shift V_0 can reach values up to 100 times the lithium recoil energy, i.e., $(V_0)_{\max}/h \approx 7.4$ MHz. Since avoiding dynamical instabilities demands $\Delta_c > \kappa$, where $\kappa/h \approx 77$ kHz is the cavity linewidth, these values, together with a typical Fermi energy of $\varepsilon_F/h \approx 10$ kHz, imply a maximal coupling of $g_{\max}/\varepsilon_F = U_0 V_0/\kappa\varepsilon_F \approx 0.2$. Using the lowest temperatures achieved in ultracold Fermi gas experiments $T/T_F \approx 0.03$ [37,38], one obtains $|g_{\max}|/4T \approx 1.7$, showing that the required regime is in principle accessible with current state-of-the-art setups. In addition, further improvements are feasible: employing cavities with reduced loss rate κ allows one to work at smaller Δ_c, and tighter mode confinement at the cavity waist increases U_0 [39]. Finally, observing the predicted ordering requires nesting between the cavity wave vector and the FS. Because the cavity-mediated interaction is of global range, such nesting requires a globally uniform density, realized in homogeneous (boxlike) traps [25,26]. To summarize, the pairing phase can be realized by combining state-of-the-art technologies for both cavity setups and boxlike traps.

Conclusions—Standing-wave or ring cavities mediate a unique type of interaction between ultracold fermions, involving the transfer of a single momentum, which can be comparable with the Fermi momentum. This property enabled us to fully solve the problem of competing Fermi-surface instabilities in such systems. We found that the superradiant density-wave instability dominates for attractive interactions but is absent in the repulsive case. There, the Fermi surface is instead gapped in a strongly momentum-dependent way by the formation of a spontaneously chosen superposition of zero- and finite-momentum fermion pairs. The corresponding temperature scales are estimated to be accessible to state-of-the-art experiments.

Note added—Recently, we became aware of Ref. [40], which focuses on superradiant density wave order and the resulting Fermi-surface reshaping, and its interplay with the Pauli crystal characterizing the Fermi gas.

Acknowledgments—B. F. acknowledges support by the DFG through the Würzburg-Dresden Cluster of Excellence on Complexity and Topology in Quantum Matter—ct.qmat (EXC 2147, project id 390858490). The work of J. L. was supported by the Deutsche Forschungsgemeinschaft (DFG, German Research Foundation) under Germany's Excellence Strategy Cluster of Excellence Matter and Light for Quantum Computing (ML4Q) EXC 2004/1 390534769, and by the DFG Collaborative Research Center (CRC) 183 Project No. 277101999. M. P. and F. P. acknowledge valuable discussions with J. P. Brantut and T. Bühler.

F. P. and B. F. conceived the study. M. P. and F. P. supervised the work. B. F. developed the theoretical framework, performed the majority of the analytic calculations, and implemented and tested the core code. M. P. generated numerical data, performed some analytic calculations, and investigated the experimental feasibility. J. L. contributed to the initial development of the code. B. F., M. P., and F. P.

wrote the original draft. All authors contributed to the interpretation of the results and to the review and editing of the manuscript.

Data availability—The data that support the findings of this article are not publicly available upon publication because it is not technically feasible and/or the cost of preparing, depositing, and hosting the data would be prohibitive within the terms of this research project. The data are available from the authors upon reasonable request.

[1] M. Y. Reizer, Phys. Rev. B **40**, 11571 (1989).
[2] F. Schlawin, D. M. Kennes, and M. A. Sentef, Appl. Phys. Rev. **9**, 011312 (2022).
[3] V. Rokaj, M. Ruggenthaler, F. G. Eich, and A. Rubio, Phys. Rev. Res. **4**, 013012 (2022).
[4] P. Rao and F. Piazza, Phys. Rev. Lett. **130**, 083603 (2023).
[5] H. Gao, F. Schlawin, M. Buzzi, A. Cavalleri, and D. Jaksch, Phys. Rev. Lett. **125**, 053602 (2020).
[6] A. Chakraborty and F. Piazza, Phys. Rev. Lett. **127**, 177002 (2021).
[7] F. Mivehvar, F. Piazza, T. Donner, and H. Ritsch, Adv. Phys. **70**, 1 (2021).
[8] F. Piazza, P. Strack, and W. Zwerger, Ann. Phys. (Amsterdam) **339**, 135 (2013).
[9] F. Piazza and P. Strack, Phys. Rev. A **90**, 043823 (2014).
[10] F. Piazza and P. Strack, Phys. Rev. Lett. **112**, 143003 (2014).
[11] J. Keeling, M. J. Bhaseen, and B. D. Simons, Phys. Rev. Lett. **112**, 143002 (2014).
[12] Y. Chen, Z. Yu, and H. Zhai, Phys. Rev. Lett. **112**, 143004 (2014).
[13] E. Colella, R. Citro, M. Barsanti, D. Rossini, and M.-L. Chiofalo, Phys. Rev. B **97**, 134502 (2018).
[14] E. Colella, S. Ostermann, W. Niedenzu, F. Mivehvar, and H. Ritsch, New J. Phys. **21**, 043019 (2019).
[15] F. Schlawin and D. Jaksch, Phys. Rev. Lett. **123**, 133601 (2019).
[16] Z. Zheng and Z. D. Wang, Phys. Rev. A **101**, 023612 (2020).
[17] X. Zhang, Y. Chen, Z. Wu, J. Wang, J. Fan, S. Deng, and H. Wu, Science **373**, 1359 (2021).
[18] V. Helson, T. Zwettler, F. Mivehvar, E. Colella, K. Roux, H. Konishi, H. Ritsch, and J.-P. Brantut, Nature (London) **618**, 716 (2023).
[19] T. Zwettler, F. Marijanović, T. Bühler, S. Chattopadhyay, G. Del Pace, L. Skolc, V. Helson, S. Uchino, E. Demler, and J.-P. Brantut, Nat. Commun. **17**, 496 (2026).
[20] Here we mean the thermodynamic limit relevant for ultracold-atom-cavity experiments, where the trap size within the cavity is large enough to be well described by a momentum continuum, while the size of the cavity itself is such that the relevant single mode is still well separated in energy from all other electromagnetic modes.
[21] T. Miyakawa, T. Sogo, and H. Pu, Phys. Rev. A **77**, 061603 (R) (2008).
[22] B. M. Fregoso and E. Fradkin, Phys. Rev. Lett. **103**, 205301 (2009).
[23] K. Aikawa, S. Baier, A. Frisch, M. Mark, C. Ravensbergen, and F. Ferlaino, Science **345**, 1484 (2014).
[24] J. Levinsen and M. M. Parish, Annu. Rev. Cold Atoms Mol. **3**, 1 (2015).
[25] K. Hueck, N. Luick, L. Sobirey, J. Siegl, T. Lompe, and H. Moritz, Phys. Rev. Lett. **120**, 060402 (2018).
[26] N. Navon, R. P. Smith, and Z. Hadzibabic, Nat. Phys. **17**, 1334 (2021).
[27] W. Zwerger, *The BCS-BEC Crossover and the Unitary Fermi Gas*, Lecture Notes in Physics (Springer, Berlin, Heidelberg, 2011).
[28] W. Zwerger, in *Quantum Matter at Ultralow Temperatures, Proceedings of the International School of Physics "Enrico Fermi", Course 191, Varenna, 7-15 July 2014*, edited by M. Inguscio, W. Ketterle, S. Stringari, and G. Roati (IOS Press, Amsterdam, 2016), pp. 63–141.
[29] S. Bux, C. Gnahm, Reinhardt A. W. Maier, C. Zimmermann, and P. W. Courteille, Phys. Rev. Lett. **106**, 203601 (2011).
[30] S. Bux, H. Tomczyk, D. Schmidt, P. W. Courteille, N. Piovella, and C. Zimmermann, Phys. Rev. A **87**, 023607 (2013).
[31] See Supplemental Material at http://link.aps.org/supplemental/10.1103/t4xb-6x3z, which includes Refs. [5–7,10,17–19,32,33], for details on the calculations.
[32] L. Rademaker, Y. Wang, T. Berlijn, and S. Johnston, New J. Phys. **18**, 022001 (2016).
[33] J. Blaizot and G. Ripka, *Quantum Theory of Finite Systems* (MIT Press, Cambridge, MA, 1986).
[34] H. Ritsch, P. Domokos, F. Brennecke, and T. Esslinger, Rev. Mod. Phys. **85**, 553 (2013).
[35] A. Altland and B. D. Simons, *Condensed Matter Field Theory* (Cambridge University Press, Cambridge, England, 2010).
[36] T. N. C. Bühler, T. Zwettler, G. S. Bolognini, A. H. Fabre, V. Y. Helson, G. D. Pace, and J.-P. Brantut, SciPost Phys. **18**, 133 (2025).
[37] N. Navon, S. Nascimbène, F. Chevy, and C. Salomon, Science **328**, 729 (2010).
[38] L. Sobirey, N. Luick, M. Bohlen, H. Biss, H. Moritz, and T. Lompe, Science **372**, 844 (2021).
[39] G. S. Bolognini, Z. Xue, M. A. Eichenberger, N. Sauerwein, F. Orsi, E. Fedotova, R. P. Bhatt, and J. P. Brantut, Opt. Express **33**, 44051 (2025).
[40] D. Ortuño Gonzalez, R. Lin, J. Stefaniak, A. Baumgärtner, G. Natale, T. Donner, and R. Chitra, Phys. Rev. Lett. **136**, 083405 (2026).

End Matter

Superradiant transition—At mean-field level, the superradiant phase transition condition can be found by imposing the closing of the gap in the cavity photon spectrum [8,10,11], which for $\Delta_c \ll \kappa$ corresponds to

$$\Delta_c = \mathrm{Re}[\Pi^R(|\boldsymbol{Q}| = Q_c, \Omega = 0)], \tag{A1}$$

where $\Pi^R(\boldsymbol{Q}, \Omega)$ is the density response of the gas given by the Lindhard function

$$\Pi^R(\boldsymbol{Q},\Omega)=\frac{2g\Delta_c N_{\mathrm{at}}}{n}\int\frac{d\boldsymbol{k}}{(2\pi)^2}\frac{n_F(\xi_{\boldsymbol{k}})-n_F(\xi_{\boldsymbol{k}+\boldsymbol{Q}})}{\Omega+\xi_{\boldsymbol{k}}-\xi_{\boldsymbol{k}+\boldsymbol{Q}}+i0^+},\tag{A2}$$

where N_{at} is the total number of atoms, n is the atomic density, and n_F is the Fermi-Dirac distribution. Performing the angular integral in Eq. (A2) and expressing the relation (A1) in dimensionless units using $\varepsilon_F=2\pi n/m$ and $k_F=\sqrt{2m\varepsilon_F}$, one obtains the condition

$$1=-8N_{\mathrm{at}}\frac{g}{\varepsilon_F}\int_0^{1/2}d\tilde{k}\frac{\tilde{k}}{\sqrt{1-4\tilde{k}^2}}n_F(\xi_{\tilde{k}}),\tag{A3}$$

where $\tilde{k}=k/k_F$. All the terms on the rhs are positive except for g, thus the condition is satisfied only for $g<0$. At $T=0$, we find that g_c scales as $1/N_{\mathrm{at}}$ (see Fig. 1).

Details on mean-field approach—This section provides further details on the extension of the mean-field approach to the entire momentum space, introduced in Eq. (4). A graphical representation of the momentum description is given in Fig. 5. To simplify the notation we define $\boldsymbol{k}^{\pm}=\boldsymbol{k}_{\mathrm{hs}}+\boldsymbol{\delta k}^{\pm}$, with $\boldsymbol{\delta k}^{\pm}=(\pm\delta k_x,\delta k_y)$. As can be seen in Fig. 5, this choice of momenta together with their mirror images conserves the $k_{x,y}\to-k_{x,y}$ mirror symmetry of the system. Moreover, we note that the full Hamiltonian $\hat{H}$ from Eq. (1) possesses a special continuous rotation symmetry in momentum space

$$\begin{pmatrix}\hat{c}_{\boldsymbol{k}^-+l\boldsymbol{Q}_c}\\ \hat{c}_{-\boldsymbol{k}^++(l+1)\boldsymbol{Q}_c}\end{pmatrix}\to\underbrace{\begin{pmatrix}\cos(\alpha)&-\sin(\alpha)\\ \sin(\alpha)&\cos(\alpha)\end{pmatrix}}_{\equiv\underline{R}(\alpha)}\begin{pmatrix}\hat{c}_{\boldsymbol{k}^-+l\boldsymbol{Q}_c}\\ \hat{c}_{-\boldsymbol{k}^++(l+1)\boldsymbol{Q}_c}\end{pmatrix},\tag{B1}$$

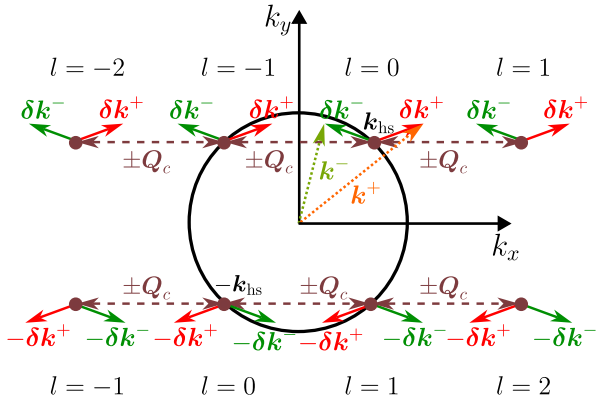

FIG. 5. Schematic representation of the momentum structure used for the mean-field decoupling. The hot spots and their mirror images are indicated by brown dots, while l gives the corresponding index. The momentum deviations $\boldsymbol{\delta k}^+$ and $\boldsymbol{\delta k}^-$ are depicted by red and green arrows.

as is evidenced in SM. Physically, this symmetry arises from the fact that any scattering process $(\boldsymbol{q}_1^{(\mathrm{in})},\boldsymbol{q}_2^{(\mathrm{in})})\to(\boldsymbol{q}_1^{(\mathrm{out})},\boldsymbol{q}_2^{(\mathrm{out})})$ has an equivalent counterpart obtained by flipping the sign of the q_y components of either $\boldsymbol{q}_1^{(\mathrm{in,out})}$ or $\boldsymbol{q}_2^{(\mathrm{in,out})}$ since $\xi_{q_x,-q_y}=\xi_{q_x,q_y}$. Since these processes are independent, they can occur in arbitrary superpositions.

Next, we construct the mean-field Hamiltonian $\hat{H}_{\mathrm{MF}}$ for the full momentum space under the condition that it is invariant under the action of $\underline{R}(\alpha)$. With the $\boldsymbol{k}^{\pm}$ notation, the generalization of Cooper pairs of Eq. (4) then becomes

$$\Delta^{(0)}_{\boldsymbol{k}^{\pm}+l\boldsymbol{Q}_c}\equiv g\langle\hat{c}_{-(\boldsymbol{k}^{\pm}+l\boldsymbol{Q}_c)}\hat{c}_{\boldsymbol{k}^{\pm}+l\boldsymbol{Q}_c}\rangle.\tag{B2}$$

Setting $l=0$ and taking the limit $\boldsymbol{\delta k}\to0$ returns the hot spots. The corresponding mean-field decoupling of the interaction Hamiltonian is given by (see [31] for details)

$$\begin{aligned}\hat{H}_{\mathrm{Cooper}}=\sum_{\substack{\delta k_x,\delta k_y\\ s=\pm1,l}}\Big[&(\bar{\Delta}^{(0)}_{\boldsymbol{k}^++(l+s)\boldsymbol{Q}_c}\hat{c}_{-(\boldsymbol{k}^++l\boldsymbol{Q}_c)}\hat{c}_{\boldsymbol{k}^++l\boldsymbol{Q}_c}+\mathrm{H.c.})\\&+g^{-1}\bar{\Delta}^{(0)}_{\boldsymbol{k}^++(l+s)\boldsymbol{Q}_c}\Delta^{(0)}_{\boldsymbol{k}^++l\boldsymbol{Q}_c}+(\boldsymbol{k}^+\leftrightarrow\boldsymbol{k}^-)\Big].\end{aligned}\tag{B3}$$

Regarding PDW states, arbitrary c.m. momenta $\boldsymbol{P}$ are, in principle, possible. In the ring-cavity setup, however, the Hamiltonian (1) conserves momentum such that PDW states with different $\boldsymbol{P}$ are decoupled. This is not valid in the case of a Fabry-Pérot cavity, where pairing sectors of different c.m. momenta mix such that all possibilities have to be taken into account, which changes the results quantitatively but leaves the overall physical picture untouched. Here, we focus on the specific generalization of the PDW expectation values [equivalent to Eq. (4)]

$$\begin{aligned}\Delta^{(+)}_{\boldsymbol{k}^++l\boldsymbol{Q}_c}&\equiv g\langle\hat{c}_{\boldsymbol{k}^--(l+1)\boldsymbol{Q}_c}\hat{c}_{\boldsymbol{k}^++l\boldsymbol{Q}_c}\rangle,\\ \Delta^{(-)}_{-\boldsymbol{k}^-+l\boldsymbol{Q}_c}&\equiv g\langle\hat{c}_{-\boldsymbol{k}^+-(l-1)\boldsymbol{Q}_c}\hat{c}_{-\boldsymbol{k}^-+l\boldsymbol{Q}_c}\rangle,\end{aligned}\tag{B4}$$

since this choice preserves the continuous rotation symmetry (B1). In particular, the corresponding decoupled Hamiltonian reads

$$\begin{aligned}\hat{H}_{\mathrm{PDW}}=\sum_{\substack{\delta k_x,\delta k_y\\ s=\pm1,l}}[&(\bar{\Delta}^{(+)}_{\boldsymbol{k}^++(l+s)\boldsymbol{Q}_c}\hat{c}_{\boldsymbol{k}^--(l+1)\boldsymbol{Q}_c}\hat{c}_{\boldsymbol{k}^++l\boldsymbol{Q}_c}\\&+\bar{\Delta}^{(-)}_{-\boldsymbol{k}^-+(l+s)\boldsymbol{Q}_c}\hat{c}_{-\boldsymbol{k}^+-(l-1)\boldsymbol{Q}_c}\hat{c}_{-\boldsymbol{k}^-+l\boldsymbol{Q}_c}+\mathrm{H.c.})\\&+g^{-1}(\bar{\Delta}^{(+)}_{\boldsymbol{k}^++(l+s)\boldsymbol{Q}_c}\Delta^{(+)}_{\boldsymbol{k}^++l\boldsymbol{Q}_c}+\bar{\Delta}^{(-)}_{-\boldsymbol{k}^-+(l+s)\boldsymbol{Q}_c}\Delta^{(-)}_{-\boldsymbol{k}^-+l\boldsymbol{Q}_c})],\end{aligned}\tag{B5}$$

while $\hat{H}_{\mathrm{Cooper}}+\hat{H}_{\mathrm{PDW}}$ remains invariant under $\underline{R}(\alpha)$ (see Ref. [31] for a proof). However, the order

parameters in the pairing sector transform as follows: $(\Delta^{(0)}_{\boldsymbol{k}^+ + l\boldsymbol{Q}_c}, \Delta^{(+)}_{\boldsymbol{k}^+ + l\boldsymbol{Q}_c}) \to \underline{R}^{-1}(\alpha)(\Delta^{(0)}_{\boldsymbol{k}^+ + l\boldsymbol{Q}_c}, \Delta^{(+)}_{\boldsymbol{k}^+ + l\boldsymbol{Q}_c})$, and $(\Delta^{(0)}_{-\boldsymbol{k}^- + l\boldsymbol{Q}_c}, \Delta^{(-)}_{-\boldsymbol{k}^- + l\boldsymbol{Q}_c}) \to \underline{R}(\alpha)(\Delta^{(0)}_{-\boldsymbol{k}^- + l\boldsymbol{Q}_c}, \Delta^{(-)}_{-\boldsymbol{k}^- + l\boldsymbol{Q}_c})$. As a consequence, the Cooper pairing and PDW states do not compete in breaking the global U(1) symmetry of $\hat{H}$ associated with the particle number conservation. Instead, the pairing instability occurs simultaneously for $\Delta^{(0,\pm)}$ by also spontaneously breaking the SO(2) symmetry of Eq. (B1). The attained value of α describes the relative admixture of Cooper and PDW pairing. This behavior is indeed observed both analytically and numerically. Finally, Eq. (B4) implies $\pm\boldsymbol{P}(\delta\boldsymbol{k}) = \pm(2\boldsymbol{k}_{\mathrm{hs}} - \boldsymbol{Q}_c + 2\delta k_y \hat{\boldsymbol{e}}_{k_y})$, such that the hot spots are again recovered for $l = 0$ and $\delta\boldsymbol{k} \to 0$.

In the exchange channel, the generalization of the XCON away from the hot spot is defined as

$$\begin{aligned} X_{\boldsymbol{k}^+ + l\boldsymbol{Q}_c} &\equiv g\langle \hat{c}^\dagger_{-\boldsymbol{k}^+ + (l+1)\boldsymbol{Q}_c} \hat{c}_{\boldsymbol{k}^+ + l\boldsymbol{Q}_c}\rangle \\ X_{\boldsymbol{k}^- + l\boldsymbol{Q}_c} &\equiv g\langle \hat{c}^\dagger_{-\boldsymbol{k}^- + l\boldsymbol{Q}_c} \hat{c}_{\boldsymbol{k}^- + (l-1)\boldsymbol{Q}_c}\rangle, \end{aligned} \tag{B6}$$

since the other option $g\langle \hat{c}^\dagger_{-\boldsymbol{k}^\pm + (l+1)\boldsymbol{Q}_c} \hat{c}_{\boldsymbol{k}^\mp + l\boldsymbol{Q}_c}\rangle$ requires the excitation of two particles or two holes. The corresponding relative momenta become $\boldsymbol{K}(\delta\boldsymbol{k}^\pm) = 2(\boldsymbol{k}_{\mathrm{hs}} + \delta\boldsymbol{k}^\pm) - \boldsymbol{Q}_c$ and we have

$$\begin{aligned} \hat{H}^{(X)}_{\mathrm{XCON}} = \sum_{\substack{\delta k_x, \delta k_y \\ s=\pm 1, l}} [&(\bar{X}_{\boldsymbol{k}^+ + (l+s)\boldsymbol{Q}_c} \hat{c}^\dagger_{-(\boldsymbol{k}^+ + (l+1)\boldsymbol{Q}_c)} \hat{c}_{\boldsymbol{k}^+ + l\boldsymbol{Q}_c} + \mathrm{H.c.}) \\ &+ g^{-1} \bar{X}_{\boldsymbol{k}^+ + (l+s)\boldsymbol{Q}_c} X_{\boldsymbol{k}^+ + l\boldsymbol{Q}_c} + (\boldsymbol{k}^+ \leftrightarrow \boldsymbol{k}^-)]. \end{aligned} \tag{B7}$$

In order to comply with the rotation symmetry (B1), we additionally have to take

$$Y_{\pm\boldsymbol{k}^+ + l\boldsymbol{Q}_c} \equiv g\langle \hat{c}^\dagger_{\pm\boldsymbol{k}^- + l\boldsymbol{Q}_c} \hat{c}_{\pm\boldsymbol{k}^+ + l\boldsymbol{Q}_c}\rangle \tag{B8}$$

into account. These expectation values describe exciton condensation around the same hot spot, which entails the smaller relative momenta $\boldsymbol{K}(\delta\boldsymbol{k}) = 2\delta k_x \hat{\boldsymbol{e}}_{k_x}$ and the mean-field interaction

$$\begin{aligned} \hat{H}^{(Y)}_{\mathrm{XCON}} = \sum_{\substack{\delta k_x, \delta k_y \\ s=\pm 1, l}} [&(\bar{Y}_{\boldsymbol{k}^+ + (l+s)\boldsymbol{Q}_c} \hat{c}^\dagger_{\boldsymbol{k}^- + l\boldsymbol{Q}_c} \hat{c}_{\boldsymbol{k}^+ + l\boldsymbol{Q}_c} + \mathrm{H.c.}) \\ &+ g^{-1} \bar{Y}_{\boldsymbol{k}^+ + (l+s)\boldsymbol{Q}_c} Y_{\boldsymbol{k}^+ + l\boldsymbol{Q}_c} + (\boldsymbol{k}^\pm \leftrightarrow -\boldsymbol{k}^\pm)]. \end{aligned} \tag{B9}$$

In this case, one finds that $\hat{H}^{(X)}_{\mathrm{XCON}} + \hat{H}^{(Y)}_{\mathrm{XCON}}$ is invariant under $\underline{R}(\alpha)$, while the order parameters transform like $(Y_{\boldsymbol{k}^+ + l\boldsymbol{Q}_c}, X_{\boldsymbol{k}^+ + l\boldsymbol{Q}_c}) \to \underline{R}(\alpha)(Y_{\boldsymbol{k}^+ + l\boldsymbol{Q}_c}, X_{\boldsymbol{k}^+ + l\boldsymbol{Q}_c})$ and $(Y_{-\boldsymbol{k}^+ + l\boldsymbol{Q}_c}, X_{\boldsymbol{k}^- + l\boldsymbol{Q}_c}) \to \underline{R}^{-1}(\alpha)(Y_{-\boldsymbol{k}^+ + l\boldsymbol{Q}_c}, X_{\boldsymbol{k}^- + l\boldsymbol{Q}_c})$. As in the pairing sector, this means that X and Y occur in a superposition and thus $T_c^{(Y)} = T_c^{(X)}$ from Eq. (7).

Finally, we also include the momentum occupation numbers, which in fact do not give rise to an instability but affect the shape of the interacting FS. The corresponding Hamiltonian contribution reads

$$\begin{aligned} \hat{H}_{\hat{n}} = -g \sum_{\substack{\delta k_x, \delta k_y \\ u, s=\pm 1, l}} [&\langle \hat{n}_{u\boldsymbol{k}^+ + (l+s)\boldsymbol{Q}_c}\rangle \hat{c}^\dagger_{u\boldsymbol{k}^+ + l\boldsymbol{Q}_c} \hat{c}_{u\boldsymbol{k}^+ + l\boldsymbol{Q}_c} \\ &- \frac{1}{2}\langle \hat{n}_{u\boldsymbol{k}^+ + (l+s)\boldsymbol{Q}_c}\rangle \langle \hat{n}_{u\boldsymbol{k}^+ + l\boldsymbol{Q}_c}\rangle + (\boldsymbol{k}^+ \leftrightarrow \boldsymbol{k}^-)]. \end{aligned} \tag{B10}$$

The total mean-field Hamiltonian $\hat{H}_{\mathrm{MF}} = \hat{H}_0 + \hat{H}_{\mathrm{Cooper}} + \hat{H}_{\mathrm{PDW}} + \hat{H}_{\hat{n}} + \hat{H}^{(X)}_{\mathrm{XCON}} + \hat{H}^{(Y)}_{\mathrm{XCON}}$, where $\hat{H}_0 = \sum_{\delta k_x, \delta k_y, u=\pm, l} [\xi_{u(\boldsymbol{k}^+ + l\boldsymbol{Q}_c)} \hat{n}_{u(\boldsymbol{k}^+ + l\boldsymbol{Q}_c)} + (\boldsymbol{k}^+ \leftrightarrow \boldsymbol{k}^-)]$ denotes the kinetic energy, can be diagonalized via a Bogoliubov transformation [33]

$$\hat{H}_{\mathrm{MF}} = \sum_\alpha \epsilon_\alpha \hat{\gamma}^\dagger_\alpha \hat{\gamma}_\alpha + E_0, \tag{B11}$$

to fermionic excitations $\hat{\gamma}_\alpha$ with positive energies ϵ_α and the mean-field ground-state energy E_0 (see Ref. [31] for details), which both depend on the order parameters. From the corresponding free energy density $\mathcal{F}_{\mathrm{MF}}$, one obtains via the thermodynamic conditions

$$\begin{aligned} &\frac{\delta\mathcal{F}_{\mathrm{MF}}}{\delta\bar{\Delta}^{(0)}_{\boldsymbol{k}^\pm + l\boldsymbol{Q}_c}} = \frac{\delta\mathcal{F}_{\mathrm{MF}}}{\delta\bar{\Delta}^{(+)}_{\boldsymbol{k}^+ + l\boldsymbol{Q}_c}} = \frac{\delta\mathcal{F}_{\mathrm{MF}}}{\delta\bar{\Delta}^{(-)}_{-\boldsymbol{k}^- + l\boldsymbol{Q}_c}} = 0, \\ &\frac{\delta\mathcal{F}_{\mathrm{MF}}}{\delta\bar{X}_{\boldsymbol{k}^\pm + l\boldsymbol{Q}_c}} = \frac{\delta\mathcal{F}_{\mathrm{MF}}}{\delta\bar{Y}_{\pm\boldsymbol{k}^+ + l\boldsymbol{Q}_c}} = 0, \\ &\frac{\delta\mathcal{F}_{\mathrm{MF}}}{\delta\overline{\langle \hat{n}_{\pm\boldsymbol{k}^\pm + l\boldsymbol{Q}_c}\rangle}} = 0, \end{aligned} \tag{B12}$$

the set of self-consistent mean-field equations:

$$\begin{aligned} \Delta^{(r)}_{\boldsymbol{q} + l\boldsymbol{Q}_c} &= -\frac{g}{2} \sum_{\alpha,\ l'} (\underline{M})^{-1}_{ll'} \mathrm{th}\left(\frac{\beta\epsilon_\alpha}{2}\right) \frac{\delta\epsilon_\alpha}{\delta\bar{\Delta}^{(r)}_{\boldsymbol{q} + l'\boldsymbol{Q}_c}}, \\ A^{(+)}_{\boldsymbol{q} + l\boldsymbol{Q}_c} &= \frac{g}{2} \sum_{\alpha,\ l'} (\underline{M})^{-1}_{ll'} \mathrm{th}\left(\frac{\beta\epsilon_\alpha}{2}\right) \frac{\delta\epsilon_\alpha}{\delta\bar{A}^{(+)}_{\boldsymbol{q} + l'\boldsymbol{Q}_c}}, \\ \langle \hat{n}_{\pm\boldsymbol{k}^\pm + l\boldsymbol{Q}_c}\rangle - \frac{1}{2} &= \frac{1}{2} \sum_{\alpha, l'} (\underline{M})^{-1}_{ll'} \mathrm{th}\left(\frac{\beta\epsilon_\alpha}{2}\right) \frac{\delta(\epsilon_\alpha/g)}{\delta\langle \hat{n}_{\pm\boldsymbol{k}^\pm + l'\boldsymbol{Q}_c}\rangle}. \end{aligned} \tag{B13}$$

Here we define the indices $(r, \boldsymbol{q}) = (0, \boldsymbol{k}^\pm), (+, \boldsymbol{k}^+), (-, -\boldsymbol{k}^-)$ for the first line and $(A, \boldsymbol{q}) = (X, \boldsymbol{k}^\pm), (Y, \pm\boldsymbol{k}^+)$ for the second line. The matrix $\underline{M}_{ll'} = \delta_{l,l'+1} + \delta_{l,l'-1}$, which takes the fixed momentum transfer into account, makes the mean-field equations resemble a nearest-neighbor tight-binding model in momentum space. This gives rise, for instance, to the sign change of $\Delta^{(0,\pm)}_{\boldsymbol{k}}$ upon shifting $\boldsymbol{k} \to \boldsymbol{k} + \boldsymbol{Q}_c$ as is depicted Fig. 3.